

# Robust, Deep and Inductive Anomaly Detection

Raghavendra Chalapathy<sup>1</sup>, Aditya Krishna Menon<sup>2</sup>, and Sanjay Chawla<sup>3</sup>

<sup>1</sup> University of Sydney and Capital Markets Cooperative Research Centre (CMCRC)

<sup>2</sup> Data61/CSIRO and the Australian National University

<sup>3</sup> Qatar Computing Research Institute (QCRI), HBKU

rcha9612@uni.sydney.edu.au, aditya.menon@data61.csiro.au, schawla@qf.org.qa

**Abstract.** PCA is a classical statistical technique whose simplicity and maturity has seen it find widespread use as an anomaly detection technique. However, it is limited in this regard by being sensitive to gross perturbations of the input, and by seeking a linear subspace that captures normal behaviour. The first issue has been dealt with by *robust PCA*, a variant of PCA that explicitly allows for some data points to be arbitrarily corrupted; however, this does not resolve the second issue, and indeed introduces the new issue that one can no longer inductively find anomalies on a test set. This paper addresses both issues in a single model, the *robust autoencoder*. This method learns a nonlinear subspace that captures the majority of data points, while allowing for some data to have arbitrary corruption. The model is simple to train and leverages recent advances in the optimisation of deep neural networks. Experiments on a range of real-world datasets highlight the model's effectiveness.

**Keywords:** anomaly detection, outlier detection, robust PCA, autoencoders

## 1 Anomaly detection: motivation and challenges

A common need when analysing real-world datasets is determining which instances stand out as being dramatically dissimilar to all others. Such instances are known as *anomalies*, and the goal of *anomaly detection* (also known as *outlier detection*) is to determine all such instances in a data-driven fashion [9]. Anomalies can be caused by errors in the data but sometimes are indicative of a new, previously unknown, underlying process; in fact Hawkins [13] defines an outlier as an observation that *deviates so significantly from other observations as to arouse suspicion that it was generated by a different mechanism*.

Principal Component Analysis (PCA) [14] is a core method for a range of statistical inference tasks, including anomaly detection. The basic idea of PCA is that while many data sets are high-dimensional, they tend to inhabit a *low-dimensional manifold*. PCA thus operates by (linearly) projecting data into a lower-dimensional space, so as to separate the *signal* from the *noise*; a data point which is far away from its projection is deemed as anomalous.

While intuitive and popular, PCA has limitations as an anomaly detection method. Notably, it is highly sensitive to anomalies: one extreme data point

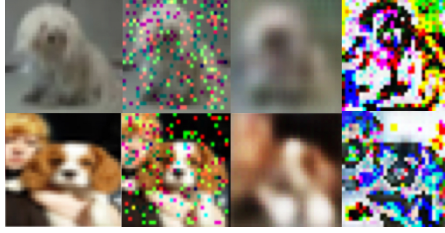


**Fig. 1.** Illustration of the noise suppression and anomaly detection capability of deep inductive convolutional autoencoders. The data set consists of “dog” images (first column) corrupted with noise (second column). Our proposed robust autoencoder decomposes an image  $\mathbf{X} = \hat{\mathbf{X}} + \mathbf{N}$ . The  $\hat{\mathbf{X}}$  (third column) shows the reconstructed image and  $\mathbf{N}$  (fourth column) shows the difference between the original and the reconstructed image. In the first row, a dog image is de-noised, while in the second row, an image of a dog with a boy (an anomaly) is poorly reconstructed.

can completely change the orientation of the projection, often leading to the masking of anomalies. A variant of PCA, known as a *robust* PCA (RPCA) limits the impact of anomalies by using a clever decomposition of the data matrix [8]. We will discuss RPCA in detail in Section 2, but note here that it still carries out a linear projection, and further cannot be used to make predictions on test instances; that is, we cannot perform *inductive* anomaly detection.

In this paper, we will relax the linear projection limitation of RPCA by using a deep and robust autoencoder [26,12]. The difference between RPCA and a deep autoencoder will be the use of a nonlinear activation function and the potential use of several hidden layers in the autoencoder.

Figure 1 shows the output of using a robust and deep autencoder to recover images. The data set consists of images of dogs where each image has been corrupted with a small amount of noise. The proposed autoencoder is able to reconstruct the dog images but fails to properly reconstruct an image which has a dog and a boy. In fact, the image of the dog with the boy was discovered as part of the anomaly detection process using autoencoders.

The rest of the paper is structured as follows. We begin with an overview of anomaly detection methods (Section 2), with a specific emphasis on matrix decomposition techniques such as PCA and its robust extensions. We then proceed to describe our proposed model based on autoencoders (Section 3), and present our experiment setup and results (Section 4,5). Finally, we describe directions for future work (Section 6).

## 2 Background and related work on anomaly detection

Consider a feature matrix  $\mathbf{X} \in \mathbb{R}^{N \times D}$ , where  $N$  denotes the number of data points and  $D$  the number of features for each point. For example,  $N$  could be the number of images in some photo collection, and  $D$  the number of pixels used to represent each image. The goal of anomaly detection is to determine which

rows of  $\mathbf{X}$  are anomalous, in the sense of being dissimilar to all other rows. We will use  $\mathbf{X}_{i:}$  to denote the  $i$ th row of  $\mathbf{X}$ .

## 2.1 A tour of anomaly detection methods

Anomaly detection is a widely researched topic in the data mining and machine learning community [9,2]. Research in this topic has focussed on either designing novel algorithms to detect anomalies, or designing *efficient* means of discovering all anomalies in a large dataset. In the latter strand, starting from the work of Bay and Schwabacher [4], several optimisations have been proposed to discover anomalies in near linear time [11].

In the former strand, which is our primary focus, much of the emphasis has been on non-parametric methods like distance and density based outliers [20,7]. For example, distance-based methods define a domain-dependent dissimilarity metric, and deem a point to be anomalous if it is relatively far away from its neighbours compared to others [29]. Another popular non-parametric approach is the one-class SVM, which learns a smooth boundary that captures the majority of probability mass of the data [24].

In recent years, with the proliferation of convex and continuous optimization methods in data mining and machine learning, matrix factorization methods for anomaly detection have become popular. We describe several popular examples of this approach, beginning with principal component analysis (PCA).

## 2.2 PCA for anomaly detection

Suppose without loss of generality that the data matrix  $\mathbf{X}$  has zero mean. Then, PCA finds the directions of maximal variance of the data, which may be understood as the result of a matrix factorisation [6]:

$$\min_{\mathbf{W}^T \mathbf{W} = \mathbf{I}, \mathbf{Z}} \|\mathbf{X} - \mathbf{WZ}\|_F^2 = \min_{\mathbf{U}} \|\mathbf{X} - \mathbf{XUU}^T\|_F^2. \quad (1)$$

Here,  $\mathbf{U} \in \mathbb{R}^{D \times K}$  for some number of *latent dimensions*  $K \ll D$ . We can interpret  $\mathbf{XU}$  as a projection (or encoding) of  $\mathbf{X}$  into a  $K$ -dimensional subspace, with the further application of  $\mathbf{U}^T$  as an inverse projection (or encoding) back into the original  $D$  dimensional space.

The matrix  $\hat{\mathbf{X}} = \mathbf{XUU}^T$  is the reconstruction of the input. One can use the norm  $\|\mathbf{X}_{i:} - \hat{\mathbf{X}}_{i:}\|_2^2$  as a measure of how anomalous a particular point  $\mathbf{X}_{i:}$  is; if the reconstruction is close to the input, then it is deemed normal; else, anomalous.

## 2.3 Autoencoders for anomaly detection

PCA assumes a linear subspace explains the data. To relax this assumption, consider instead

$$\min_{\mathbf{U}, \mathbf{V}} \|\mathbf{X} - f(\mathbf{XU})\mathbf{V}\|_F^2 \quad (2)$$

for some non-decreasing *activation function*  $f: \mathbb{R} \rightarrow \mathbb{R}$ , and  $\mathbf{U} \in \mathbb{R}^{D \times K}$ ,  $\mathbf{V} \in \mathbb{R}^{K \times D}$ . This objective corresponds to an autoencoder with a single hidden layer [12]. Popular choices of  $f(\cdot)$  include the sigmoid  $f(a) = (1 + \exp(-a))^{-1}$  and the rectified linear unit or ReLU  $f(x) = \max(0, a)$ . As before, we can interpret  $\mathbf{XU}$  as an encoding of  $\mathbf{X}$  into a  $K$ -dimensional subspace; however, by applying a nonlinear  $f(\cdot)$ , the projection is implicitly into a nonlinear subspace.

For the purposes of anomaly detection, one can define the reconstruction matrix  $\hat{\mathbf{X}} = f(\mathbf{XU})\mathbf{V}$ . Then, as before, one can use the norm  $\|\mathbf{X}_{i:} - \hat{\mathbf{X}}_{i:}\|_2^2$  as a measure of how anomalous a particular data point  $\mathbf{X}_{i:}$  is. Compared to PCA, one learns a *nonlinear* manifold that best captures the data.

## 2.4 Robust PCA for anomaly detection

Another way to generalise PCA is to solve, for a tuning parameter  $\lambda > 0$ ,

$$\min_{\mathbf{S}, \mathbf{N}} \|\mathbf{S}\|_* + \lambda \cdot \|\mathbf{N}\|_1 : \mathbf{X} = \mathbf{S} + \mathbf{N}, \quad (3)$$

where  $\|\cdot\|_*$  denotes the trace or nuclear norm  $\|\mathbf{X}\|_* = \text{tr}((\mathbf{X}^T \mathbf{X})^{1/2})$ , and  $\|\cdot\|_1$  the elementwise  $\ell_1$  norm. Intuitively, this separates  $\mathbf{X}$  into a signal matrix  $\mathbf{S}$  and a noise matrix  $\mathbf{N}$ , where the signal matrix has low-rank structure, and the noise is assumed to not overwhelm the signal for most of the matrix entries. The trace norm may be seen as a convex relaxation of the rank function; thus, this objective can be understood as a relaxed version of PCA.

For the purposes of anomaly detection, one can define the reconstruction matrix  $\hat{\mathbf{X}} = \mathbf{X} - \mathbf{N} = \mathbf{S}$ . Then, as before, one can use the norm  $\|\mathbf{X}_{i:} - \hat{\mathbf{X}}_{i:}\|_2^2 = \|\mathbf{N}_{i:}\|_2^2$  as a measure of how anomalous a particular data point  $\mathbf{X}_{i:}$  is.

Equation 3 corresponds to robust PCA (RPCA) [8]. Observe that unlike standard PCA, this objective can effortlessly deal with a single entry perturbed arbitrarily. Observe that when  $\lambda \rightarrow +\infty$ , we will end up with  $\mathbf{N} = \mathbf{0}$ ,  $\mathbf{S} = \mathbf{X}$ , i.e. we will claim that there is no noise in the data, and so all points are deemed normal. On the other hand, when  $\lambda \rightarrow 0$ , we will end up with  $\mathbf{N} = \mathbf{X}$ ,  $\mathbf{S} = \mathbf{0}$ , i.e. we will claim that there is no signal in the data, and so points with high norm are deemed anomalous.

## 2.5 Direct robust matrix factorization

Building upon RPCA, Xiong et. al. [27] introduced the direct robust matrix factorization method (DRMF), where for tuning parameters  $K, e$  one solves:

$$\begin{aligned} \min_{\mathbf{S}, \mathbf{N}} \quad & \|\mathbf{X} - (\mathbf{N} + \mathbf{S})\|_F^2 \\ & \text{rank}(\mathbf{S}) \leq K \\ & \|\mathbf{N}\|_0 \leq e. \end{aligned} \quad (4)$$

As before, the matrix  $\mathbf{N}$  captures the anomalies and  $\mathbf{S}$  captures the signal. Unlike RPCA, one explicitly constraints  $\mathbf{S}$  to be low-rank, rather than merely having low trace norm; and one explicitly constraints  $\mathbf{N}$  to have a maximal number of nonzeros, rather than merely having bounded  $\ell_1$  norm.

### 3 From robust PCA to robust (convolutional) autoencoders

We now present our robust (convolutional) autoencoder model for anomaly detection. The method can be seen as an extension of robust PCA to allow for a nonlinear manifold that explains most of the data.

#### 3.1 Robust (convolutional) autoencoders

Let  $f: \mathbb{R} \rightarrow \mathbb{R}$  be some non-decreasing activation function. Now consider the following objective, which may be seen as combining the salient elements of Equations 2 and 3:

$$\min_{\mathbf{U}, \mathbf{V}, \mathbf{N}} \|\mathbf{X} - (f(\mathbf{X}\mathbf{U})\mathbf{V} + \mathbf{N})\|_F^2 + \frac{\mu}{2} \cdot (\|\mathbf{U}\|_F^2 + \|\mathbf{V}\|_F^2) + \lambda \cdot \|\mathbf{N}\|_1, \quad (5)$$

where  $f(\cdot)$  is understood to act elementwise. This can be considered a form of *robust autoencoder*: one encodes the input into the latent representation  $\mathbf{Z} = f(\mathbf{X}\mathbf{U})$ , which is then decoded via  $\mathbf{V}$ . The additional  $\mathbf{N}$  term captures gross outliers in the data, as with robust PCA.

When  $\lambda \rightarrow +\infty$ , we will find  $\mathbf{N} = \mathbf{0}$ , and the model reduces to a standard autoencoder (Equation 2). When  $\lambda \rightarrow 0$ , then one possible solution is  $\mathbf{N} = \mathbf{X}$  and  $\mathbf{U} = \mathbf{V} = \mathbf{0}$ , so that the model memorises the training data. For intermediate  $\lambda$ , the model augments a standard autoencoder with a noise absorption term that endows robustness.

More generally, Equation 5 can be seen as an instance of

$$\min_{\theta, \mathbf{N}} \|\mathbf{X} - (\hat{\mathbf{X}}(\theta) + \mathbf{N})\|_F^2 + \frac{\mu}{2} \cdot \Omega(\theta) + \lambda \cdot \|\mathbf{N}\|_1, \quad (6)$$

where  $\hat{\mathbf{X}}(\theta)$  is some generic predictor with parameters  $\theta$ , and  $\Omega(\cdot)$  a regularisation function. Observe that we could pick  $\hat{\mathbf{X}}(\theta)$  to be a convolutional autoencoder [18, 26], which would be suitable when dealing with image data; such a model will be studied extensively in our experiments. Further, the regulariser  $\Omega$  could involve more general matrix norms, such as the  $\ell_{1,2}$  norm [15].

While the use of deep autoencoders for denoising data is widespread, their use for anomaly detection is limited [26]. In fact to the best of our knowledge there is no published work that proposes a deep autoencoder with the an  $L_1$  decomposition. Our contribution can be seen as a non-linear extension of RPCA.

#### 3.2 Training the model

The objective function of the model of Equation 5, 6 is non-convex, but unconstrained and sub-differentiable. There are in principle several ways of performing optimisation. For example, for  $f$  differentiable, one could compute sub-gradients with respect to all model parameters and apply backpropagation. However, we observe the following:

- For fixed  $\mathbf{N}$ , the objective is equivalent to that of a standard (convolutional) autoencoder on the matrix  $\mathbf{X} - \mathbf{N}$ . Thus, one can optimise the parameters  $\theta$  using any modern (stochastic) optimisation tool for deep learning that exploits gradients, such as Adam [19].
- For fixed  $\theta$  (i.e.  $\mathbf{U}, \mathbf{V}$  in the standard autoencoder case), the objective is

$$\min_{\theta, \mathbf{N}} \|\mathbf{N} - (\mathbf{X} - \hat{\mathbf{X}}(\theta))\|_F^2 + \lambda \cdot \|\mathbf{N}\|_1,$$

which is trivially solvable via the soft thresholding operator on the matrix  $\mathbf{X} - \hat{\mathbf{X}}(\theta)$  [3], with solution

$$\mathbf{N}_{ij} = \begin{cases} (\mathbf{X} - \hat{\mathbf{X}}(\theta))_{ij} - \frac{\lambda}{2} & \text{if } (\mathbf{X} - \hat{\mathbf{X}}(\theta))_{ij} > \frac{\lambda}{2} \\ (\mathbf{X} - \hat{\mathbf{X}}(\theta))_{ij} + \frac{\lambda}{2} & \text{if } (\mathbf{X} - \hat{\mathbf{X}}(\theta))_{ij} < -\frac{\lambda}{2} \\ 0 & \text{else.} \end{cases}$$

We thus alternately optimise  $\mathbf{N}$  and  $\theta$  until the change in the overall objective is below some threshold.

We note that the use of stochastic optimisation for the first step, and the simplicity of the optimisation for the second step, means that we can easily train the model where data arrives in an online or streaming fashion.

### 3.3 Predicting with the model

One convenient property of our model is that the anomaly detector will be inductive, i.e. it can generalise to unseen data points. One can interpret the model as learning a robust representation of the input, which is unaffected by gross noise; such a representation should thus be able to accurately model any unseen points that lie on the same manifold as the data used to train the model.

Formally, given a new  $\mathbf{x}_* \in \mathbb{R}^D$ , one simply needs to compute  $f(\mathbf{x}_*^T \mathbf{U}) \mathbf{V}$  to score this point. The larger  $\|\mathbf{x}_* - \mathbf{V}^T f(\mathbf{U}^T \mathbf{x}_*)\|_2^2$  is, the more likely the point is deemed to be anomalous. We emphasise that such inductive predictions are simply not possible with the robust PCA method, as it estimates parameters for the  $N \times D$  observations present in  $\mathbf{X}$ , with no means of generalising to unseen data.

### 3.4 Connection to robust PCA

We show how the robust autoencoder can be naturally derived as an extension of robust PCA. The trace norm can be represented in the variational form [23]

$$\|\mathbf{S}\|_* = \min_{\mathbf{W}, \mathbf{V}: \mathbf{WV} = \mathbf{S}} \frac{1}{2} \cdot (\|\mathbf{W}\|_F^2 + \|\mathbf{V}\|_F^2).$$

The robust PCA objective is thus equivalently

$$\min_{\mathbf{W}, \mathbf{V}, \mathbf{N}} \frac{1}{2} \cdot (\|\mathbf{W}\|_F^2 + \|\mathbf{V}\|_F^2) + \lambda \cdot \|\mathbf{N}\|_1 : \mathbf{X} = \mathbf{WV} + \mathbf{N}.$$

This objective has the disadvantage of being non-convex, but the advantage of being amenable to extensions. Pick some  $\mu > 0$ , and consider a relaxed version of the robust PCA objective:

$$\min_{\mathbf{W}, \mathbf{V}, \mathbf{N}, \mathbf{E}} \|\mathbf{E}\|_F^2 + \frac{\mu}{2} \cdot (\|\mathbf{W}\|_F^2 + \|\mathbf{V}\|_F^2) + \lambda \cdot \|\mathbf{N}\|_1 : \mathbf{X} = \mathbf{WV} + \mathbf{N} + \mathbf{E}.$$

Here, we allow for further systematic errors  $\mathbf{E}$  which have low average magnitude. We can equally consider the unconstrained objective

$$\min_{\mathbf{W}, \mathbf{V}, \mathbf{N}} \|\mathbf{X} - (\mathbf{WV} + \mathbf{N})\|_F^2 + \frac{\mu}{2} \cdot (\|\mathbf{W}\|_F^2 + \|\mathbf{V}\|_F^2) + \lambda \cdot \|\mathbf{N}\|_1 \quad (7)$$

This re-expression of robust PCA has been previously noted, for example in Sprechmann et al. [25].

To derive the robust autoencoder from Equation 7, suppose now that we constrain  $\mathbf{W} = \mathbf{XU}$ . This is a natural constraint in light of Equation 1, since for standard PCA we factorise  $\mathbf{X}$  into  $\hat{X} = \mathbf{XUU}^T$ . Then, we have the objective

$$\min_{\mathbf{U}, \mathbf{V}, \mathbf{N}} \|\mathbf{X} - (\mathbf{XUV} + \mathbf{N})\|_F^2 + \frac{\mu}{2} \cdot (\|\mathbf{XU}\|_F^2 + \|\mathbf{V}\|_F^2) + \lambda \cdot \|\mathbf{N}\|_1.$$

Now suppose we modify the regulariser to only operate on  $\mathbf{U}$  rather than  $\mathbf{XU}$ :

$$\min_{\mathbf{U}, \mathbf{V}, \mathbf{N}} \|\mathbf{X} - (\mathbf{XUV} + \mathbf{N})\|_F^2 + \frac{\mu}{2} \cdot (\|\mathbf{U}\|_F^2 + \|\mathbf{V}\|_F^2) + \lambda \cdot \|\mathbf{N}\|_1.$$

This is again natural in the context of standard PCA, since there we have  $\mathbf{W} = \mathbf{XU}$  satisfying  $\mathbf{W}^T \mathbf{W} = \mathbf{I}$ . Observe now that we have derived Equation 5 for a linear activation function  $f(x) = x$ . The robust autoencoder thus extends this model by employing a nonlinear activation.

## 4 Experimental setup

In this section we show the empirical effectiveness of Robust Convolutional Autoencoders (RCAE) over the state-of-the-art methods on real-world data .

### 4.1 Methods compared

We show the empirical effectiveness of our proposed Robust Convolutional Autoencoders (RCAE) on a range of real-world data sets by comparing with following state-of-the art methods for anomaly detection:

- **Truncated SVD** [22], which for zero-mean features is equivalent to performing standard PCA.
- **Robust PCA (RPCA)** [8], as per Equation 3.
- **Autoencoder (AE)** [5], as per Equation 2.
- **Convolutional Autoencoders (CAE)**, a convolutional autoencoder without any accounting for gross anomalies i.e. Equation 6 where  $\lambda = +\infty$ .
- **Robust Convolutional Autoencoders (RCAE)**, our proposed model as per Equation 6.

To facilitate the replication of our experimental results, we have used TensorFlow [1] for the implementation of AE, CAE and RCAE<sup>4</sup>. For RPCA, a publicly available implementation<sup>5</sup> based on the inexact augmented Lagrange multiplier method is utilized.

## 4.2 Datasets

We compare all methods on three real-world datasets, including those used in the original robust PCA paper [8]:

- **CIFAR-10** [21] consisting of 60000  $32 \times 32$  colour images in 10 classes, with 6000 images per class.
- **usps**, comprising the USPS handwritten digits [16].
- **restaurant**, comprising video background modelling and activity detection consisting of snapshots of restaurant activities [27]

For each dataset, we perform further processing to create a well-posed anomaly detection task, as described in the next section.

## 4.3 Evaluation methodology

As anomaly detection is an unsupervised learning problem, model evaluation is challenging. We follow a standard protocol (see e.g. [27]) wherein anomalies are explicitly identified in the training set. We can then evaluate the classification performance of each method as measured against the ground truth anomaly labels. We specifically focus on three means of evaluating each method, which compare the predicted anomaly scores to the ground truth labels:

- the area under the precision-recall curve (AUPRC)
- the area under the ROC curve (AUROC)
- the precision at 10 (P@10).

For **CIFAR-10**, the dataset for comparing methods is created by combining 5000 images of dogs and 50 images of cats; a good anomaly detection method should thus flag the cats to be anomalous. Similarly, for **usps**, the dataset is created by a mixture of 220 images of ‘1’s, and 11 images of ‘7’s as in [28]. For the **restaurant** dataset, there are no ground truth anomalies, and so we perform a qualitative analysis by visually comparing the anomalies flagged by various methods, as done in the original robust PCA paper [8]. Details of the datasets are summarised in Table 1.

In addition to these comparisons of detection performance, we also test the ability of our model to perform denoising of images, as well as detecting inductive anomalies.

<sup>4</sup> <https://github.com/raghavchalapathy/rcae>

<sup>5</sup> [http://perception.csl.illinois.edu/matrix-rank/sample\\_code.html](http://perception.csl.illinois.edu/matrix-rank/sample_code.html)



Dataset	# of instances	# of anomalies	# of features
CIFAR-10	5000	50 (cats)	1024
usps	231	11 ('7')	256
restaurant	200	Unknown	19200

**Table 1.** Summary of datasets used in experiments.

#### 4.4 Network parameters

Although we have observed that deeper RCAE networks tend to achieve better image reconstruction performance, there exist four fold options related to network parameters to be chosen. We carried out anomaly detection experiments by optimally adjusting (a) number of convolutional filters, (b) filter size, (c) strides of convolution operation and (d) activation applied, to produce least reconstruction error for each of the datasets appropriately. The experiments have been run over a range of values chosen for the hyper-parameters. The hyper-parameters include the number of hidden-layer nodes,  $H \in \{3, 64, 128\}$ ,  $\lambda$  within range  $[0, 100]$ . Three additional parameters, the learning, drop-out rates and  $\mu$  the regularization parameter were sampled from a uniform distribution in the range  $[0.05, 0.1]$ . The embedding and initial weight matrices were all sampled from the uniform distribution within range  $[-1, 1]$ .

## 5 Experimental results

In this section, we present experiments conducted for three scenarios: (a) (non-inductive) anomaly detection, (b) inductive anomaly detection, and (c) image denoising.

### 5.1 Anomaly detection results

We present results on the three datasets described in Section 4. Table 2 summarises the performance for all the methods on the CIFAR-10 and usps datasets.

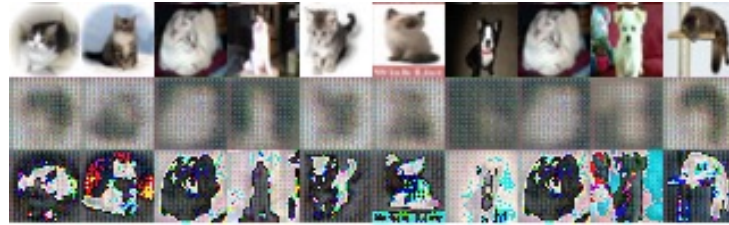
Methods	CIFAR-10			USPS		
	AUPRC	AUROC	P@10	AUPRC	Recall	P@10
RCAE	0.9934 $\pm$ 0.0003	0.6255 $\pm$ 0.0055	0.8716 $\pm$ 0.0005	0.9614 $\pm$ 0.0025	0.9988 $\pm$ 0.0243	0.9108 $\pm$ 0.0113
CAE	0.9011 $\pm$ 0.0000	0.6191 $\pm$ 0.0000	0.0000 $\pm$ 0.0000	0.7003 $\pm$ 0.0105	0.9712 $\pm$ 0.0002	0.8730 $\pm$ 0.0023
AE	0.9341 $\pm$ 0.0029	0.5260 $\pm$ 0.0003	0.2000 $\pm$ 0.0003	0.8533 $\pm$ 0.0023	0.9927 $\pm$ 0.0022	0.8108 $\pm$ 0.0003
DRMF	0.0034 $\pm$ 0.0000	0.4847 $\pm$ 0.0000	0.0000 $\pm$ 0.0000	0.7737 $\pm$ 0.0351	0.9928 $\pm$ 0.0027	0.7150 $\pm$ 0.0342
RPCA	0.0036 $\pm$ 0.0000	0.5211 $\pm$ 0.0000	0.0000 $\pm$ 0.0000	0.7893 $\pm$ 0.0195	0.9942 $\pm$ 0.0012	0.7250 $\pm$ 0.0323
SVD	0.0024 $\pm$ 0.0000	0.5299 $\pm$ 0.0000	0.0000 $\pm$ 0.0000	0.6091 $\pm$ 0.1263	0.9800 $\pm$ 0.0105	0.5600 $\pm$ 0.0249

**Table 2.** Performance comparison between the baseline (bottom three lines) and state-of-the-art systems (top three lines) over CIFAR-10 and usps. Results are the mean and standard error of performance metrics over 20 random training set draws. Highlighted cells indicate best performer.

(1) **CIFAR-10 dataset** We create a dataset with anomalies by combining 5000 random images of dogs and 50 images of cats, as illustrated in Figure 2. In this scenario the cats are anomalies, and the goal is to detect all the cats in an unsupervised way using anomaly detection methods.

**Parameter settings.** For SVD and RPCA methods, rank  $K = 64$  is used. We trained a three-hidden-layer autoencoder (AE) (1024-256-64-256-1024 neurons). The middle hidden layer size is set to be same as rank  $K = 64$  (same as number of components used in SVD and RPCA), and the model is trained using Adam [19] (adaptive moment estimation). The decoding layer uses sigmoid function in order to capture the nonlinearity characteristics from latent representations produced by the hidden layer. Finally, we obtain the feature vector for each image by obtaining the latent representation from the hidden layer.

Following the success of the Batch Normalization [17] architecture and adoption of deep network learning by Exponential Linear Units [10], have demonstrated experimentally that convolutional+batch-normalization+elu layers provide a better representation of convolutional filters. Hence, in this experiment the RCAE adopts four layers of (conv-batch-normalization-elu) in the encoder part and four layers of (conv-batch-normalization-elu) in the decoder portion of the network. RCAE network parameters such as (number of filter, filter size, strides) are chosen to be (16,3,1) for first and second layers and (32,3,1) for third and fourth layers of both encoder and decoder layers.



(a) RCAE.



(b) RPCA.

**Fig. 2.** Top 10 most anomalous images, along with background and foreground, CIFAR-10 dataset.

**Results.** From Table 2, RCAE clearly outperforms all existing state-of-the-art methods in anomaly detection. Note that basic CAE, with no robustness (effectively  $\lambda = \infty$ ), is also outperformed by our method, indicating that it is crucial to explicitly handle anomalies with the  $\mathbf{N}$  term.

Figure 2 illustrates the most anomalous images for our RCAE method, compared to RPCA. Owing to the latter involving learning a linear subspace, the model is unable to effectively distinguish cats from dogs; by contrast, RCAE can effectively determine the manifold characterising most dogs, and identifies cats to be anomalous with respect to this.

**(2) USPS dataset** From the `usps` handwritten digit dataset, we create an anomalous dataset as in [28], with a mixture of 220 images of ‘1’s, and 11 images of ‘7’. Intuitively, the latter images are treated as being anomalous, as the corresponding images have different characteristics to the majority of the training data. Each image is flattened as a row vector, yielding a  $231 \times 256$  training set matrix.

**Parameter settings.** For SVD and RPCA methods, rank  $K = 64$  is used. The input to AE are flattened images as a column vector of size 256. The hidden layer of the autoencoder is a column vector of size 64 (matching the rank  $K = 64$  used in SVD and RPCA).

For RCAE, we set two layers of convolution layers with the filter number to be 32, filter size to be  $3 \times 3$ , with number of strides as 1 and rectified linear unit (ReLU) as activation with max-pooling layer of dimension  $2 \times 2$ .

**Results.** From Table 2, we see that it is a near certainty for all ‘7’s are accurately identified as outliers. Figure 3 shows the top anomalous images for RCAE, where indeed we see that the ‘7’s are correctly placed at the top of the list.

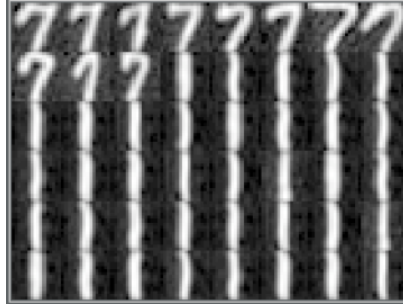


**Fig. 3.** Top anomalous images for RCAE, `usps` dataset.

**(3) Results on restaurant dataset** In this experiment we consider the joint problem of modelling the background of videos and detecting anomalous images. Estimating the background in videos is important for computer vision tasks such

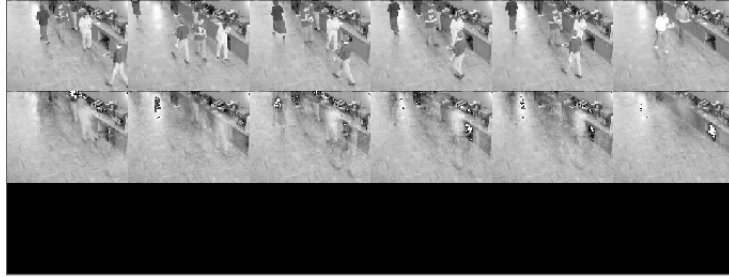
as anomalous activity detection. It is however difficult because of the variability of the background (e.g. due to lighting conditions) and the presence of foreground objects such as moving objects and people. We evaluate various methods on the **restaurant** video activity detection dataset [27]. This dataset explicitly labels pixels as belonging to the foreground or background. We treat the background images as being normal, and the foreground images as being anomalous.

**Parameter settings.** For SVD and RPCA, rank  $K = 64$  is used. We trained a three-hidden-layer autoencoder (AE) (19200-256-64-256-19200 neurons).

RCAE architecture in this experiment is same as the one adopted for CIFAR-10 dataset, containing four layers of (conv-batch-normalization-elu) in the encoder part and four layers of (conv-batch-normalization-elu) in the decoder portion of the network. RCAE network parameters such as (number of filter, filter size, strides) are chosen to be (16,3,1) for first and second layers and (32,3,1) for third and fourth layers of both encoder and decoder.



(a) RCAE.



(b) RPCA.

**Fig. 4.** Illustrates Top 10 worst reconstructed images containing original image (people walking in the lobby) decomposed into background image (lobby) and foreground (people).

**Results.** While there are no ground truth anomalies in this dataset, a qualitative analysis reveals RCAE to outperform its counterparts in capturing the foreground objects. Figure 4 compares the top 6 most anomalous images for RCAE and RPCA. We see that the most anomalous images contain high fore-

ground activity (which are recognised as anomalous). Visually, we see that the background reconstruction produced by RPCA contains a few blemishes in some cases, while for RCAE the backgrounds are smooth.

## 5.2 Inductive anomaly detection results

We conduct an experiment to assess the detection of *inductive* anomalies. Recall that this is a capability of our RCAE model, but not e.g. RPCA. We consider the following setup: we train our model on 5000 dog images, and then evaluate it on a test set comprising 500 dogs and 50 cat images. As before, we wish all methods to accurately determine the cats to be anomalies.

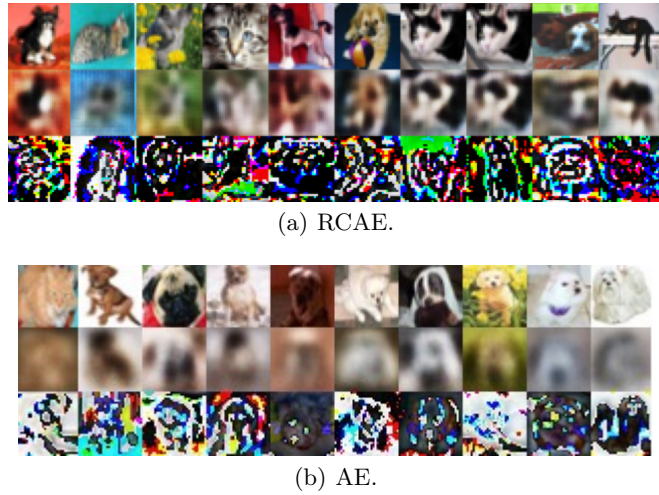


**Fig. 5.** Top 10 most anomalous images for inductive anomalies detection in `cifar-10` containing cats (anomalies) decomposed into background foreground images.

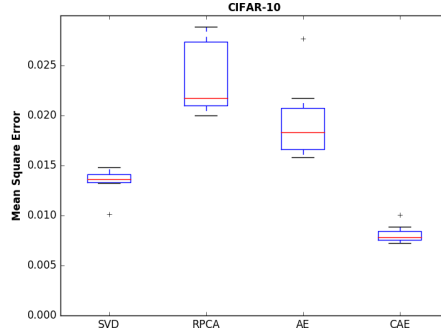
Table 3 summarises the detection performance for all the methods on this inductive task. The lower values compared to Table 2 are indicative that the problem here is more challenging than anomaly detection on a single dataset; nonetheless, we see that our RCAE method manages to convincingly outperform both the SVD and AE baselines. This is confirmed qualitatively in Figure 5, where we see that RCAE correctly identifies many cats in the test set as anomalous, while the basic AE method suffers.

## 5.3 Image denoising results

Finally, we test the ability of the model to de-noise images, which is a form of anomaly detection on individual pixels (or more generally, features). In this experiment, we train all models on a set of 5000 images of dogs from `CIFAR-10`.

**Table 3.** Inductive anomaly detection results on CIFAR-10. Highlighted cells indicate best performer.

	SVD	RPCA	DRMF	AE	CAE	RCAE
<b>AUPRC</b>	0.1752 $\pm$ 0.0051	N/A	N/A	0.6200 $\pm$ 0.0005	0.6423 $\pm$ 0.0005	0.6908 $\pm$ 0.0001
<b>AUROC</b>	0.4997 $\pm$ 0.0066	N/A	N/A	0.5007 $\pm$ 0.0010	0.4708 $\pm$ 0.0003	0.5576 $\pm$ 0.0005
<b>P@10</b>	0.2150 $\pm$ 0.0310	N/A	N/A	0.1086 $\pm$ 0.0001	0.2908 $\pm$ 0.0001	0.5986 $\pm$ 0.0001

**Fig. 6.** Illustration of the mean square error boxplots obtained for various models on image denoising task, CIFAR-10 dataset. In this setting, RCAE suppresses the noise and detects the background and foreground images effectively.

For each image, we then add salt-and-pepper noise at a rate of 10%. Our goal is to recover the original image as accurately as possible.

Figure 6 illustrates for various methods the mean square error between the reconstructed and original images. In this setting, RCAE suppresses the noise as evident from the low error, and further illustrated in Figure 7. From this figure, we also see that the most anomalous images in the presence of noise contain images of the variations of dog class images (e.g. containing person’s face).

## 6 Conclusion

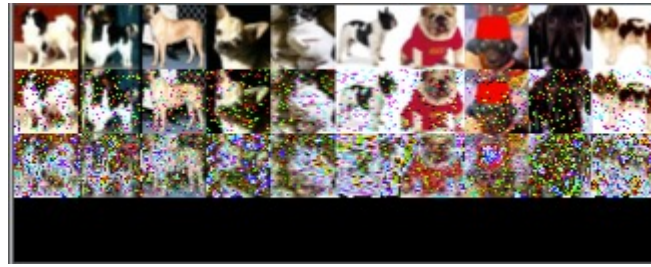
We have extended the robust PCA model to the nonlinear autoencoder setting. The robustness of the model ensures that model is not oversensitive to anomalies and the nonlinearity helps discover potentially more subtle anomalies. Furthermore our approach can be used in an inductive setting while the robust PCA cannot. The advantage of inductive anomaly detection is that it makes it possible to deploy our model in a live setting. To the best of our knowledge ours is the first approach which is both *robust* and *inductive*.

While autoencoders are a powerful mechanism for data representation they suffer from their “black-box” nature. There is a growing body of research on outlier description, i.e., explain the reason why a data point is anomalous. A direction of future reason is to extend deep autoencoders for outlier description.





(a) RCAE.



(b) RPCA.

**Fig. 7.** Top 10 most anomalous images, along with background and foreground, image denoising task on `cifar-10`.

## References

1. Abadi, M., Agarwal, A., Barham, P., Brevdo, E., Chen, Z., Citro, C., Corrado, G.S., Davis, A., Dean, J., Devin, M., et al.: Tensorflow: Large-scale machine learning on heterogeneous distributed systems. arXiv preprint arXiv:1603.04467 (2016)
2. Aggarwal, C.C.: Outlier analysis second edition (2016)
3. Bach, F., Jenatton, R., Mairal, J., Obozinski, G.: Convex Optimization with Sparsity-Inducing Norms. In: Optimization for Machine Learning, MIT Press (2011)
4. Bay, S.D., Schwabacher, M.: Mining distance-based outliers in near linear time with randomization and a simple pruning rule. In: Proceedings of Ninth ACM SIGKDD International Conference on Knowledge Discovery and Data Mining, Washington, D.C. USA. pp. 29–38 (2003)
5. Bengio, Y., et al.: Learning deep architectures for ai. Foundations and trends® in Machine Learning 2(1), 1–127 (2009)
6. Bishop, C.M.: Pattern Recognition and Machine Learning. Springer (2006)
7. Breunig, M.M., Kriegel, H.P., Ng, R.T., Sander, J.: Lof: identifying density-based local outliers. In: ACM sigmod record. vol. 29, pp. 93–104. ACM (2000)
8. Candés, E., Li, X., Ma, Y., Wright, J.: Robust principal component analysis?: Recovering low-rank matrices from sparse errors. In: Sensor Array and Multichannel Signal Processing Workshop (SAM), 2010 IEEE. pp. 201–204. IEEE (2010)
9. Chandola, V., Banerjee, A., Kumar, V.: Outlier detection: A survey. ACM Computing Surveys (2007)

10. Clevert, D.A., Unterthiner, T., Hochreiter, S.: Fast and accurate deep network learning by exponential linear units (elus). arXiv preprint arXiv:1511.07289 (2015)
11. Ghoting, A., Parthasarathy, S., Otey, M., Ghoting, A., Parthasarathy, S., Otey, M.E.: Fast mining of distance-based outliers in high-dimensional datasets. *Data Mining and Knowledge Discovery* 16(3), 349–364 (Jun 2008)
12. Goodfellow, I., Bengio, Y., Courville, A.: *Deep Learning*. MIT Press (2016), <http://www.deeplearningbook.org>
13. Hawkins, D.: *Identification of Outliers*. Chapman and Hall, London (1980)
14. Hotelling, H.: Analysis of a complex of statistical variables into principal components. *J. Educ. Psych.* 24 (1933)
15. Huang, J., Zhang, T.: The benefit of group sparsity. *Ann. Statist.* 38(4), 1978–2004 (08 2010)
16. Hull, J.J.: A database for handwritten text recognition research. *IEEE Transactions on pattern analysis and machine intelligence* 16(5), 550–554 (1994)
17. Ioffe, S., Szegedy, C.: Batch normalization: Accelerating deep network training by reducing internal covariate shift. arXiv preprint arXiv:1502.03167 (2015)
18. Jain, V., Seung, S.: Natural image denoising with convolutional networks. In: Koller, D., Schuurmans, D., Bengio, Y., Bottou, L. (eds.) *Advances in Neural Information Processing Systems* 21, pp. 769–776 (2008)
19. Kingma, D., Ba, J.: Adam: A method for stochastic optimization. arXiv preprint arXiv:1412.6980 (2014)
20. Knorr, E.M., Ng, R.T.: A unified notion of outliers: Properties and computation. In: *KDD*. pp. 219–222 (1997)
21. Krizhevsky, A., Hinton, G.: Learning multiple layers of features from tiny images (2009)
22. Pedregosa, F., Varoquaux, G., Gramfort, A., Michel, V., Thirion, B., Grisel, O., Blondel, M., Prettenhofer, P., Weiss, R., Dubourg, V., et al.: Scikit-learn: Machine learning in python. *Journal of Machine Learning Research* 12(Oct), 2825–2830 (2011)
23. Recht, B., Fazel, M., Parrilo, P.A.: Guaranteed minimum-rank solutions of linear matrix equations via nuclear norm minimization. *SIAM review* 52(3), 471–501 (2010)
24. Scholkopf, B., Platt, J.C., Shawe-Taylor, J.C., Smola, A.J., Williamson, R.C.: Estimating the support of a high-dimensional distribution. *Neural Computation* 13(7), 1443–1471 (Jul 2001)
25. Sprechmann, P., Bronstein, A.M., Sapiro, G.: Learning efficient sparse and low rank models. *IEEE Transactions on Pattern Analysis and Machine Intelligence* 37(9), 1821–1833 (Sept 2015)
26. Vincent, P., Larochelle, H., Lajoie, I., Bengio, Y., Manzagol, P.A.: Stacked denoising autoencoders: Learning useful representations in a deep network with a local denoising criterion. *The Journal of Machine Learning Research* 11, 3371–3408 (2010)
27. Xiong, L., Chen, X., Schneider, J.: Direct robust matrix factorization for anomaly detection. In: *Data Mining (ICDM), 2011 IEEE 11th International Conference on*. pp. 844–853. IEEE (2011)
28. Xu, H., Caramanis, C., Sanghavi, S.: Robust pca via outlier pursuit. In: *Advances in Neural Information Processing Systems*. pp. 2496–2504 (2010)
29. Zhao, M., Saligrama, V.: Anomaly detection with score functions based on nearest neighbor graphs. In: *Advances in Neural Information Processing Systems (NIPS)*. pp. 2250–2258 (2009)